Code-to-code Comparison for a PbLi Mixed-convection MHD Flow

S. Smolentsev,[a*] T. Rhodes,[a] Y. Yan,[a] A. Tassone,[b] C. Mistrangelo,[c] L. Bühler,[c] F. R. Urgorri[d]

[a]University of California - Los Angeles (UCLA), USA
[b]University of Rome, Italy
[c]Karlsruhe Institute of Technology (KIT), Germany
[d]Centre for Energy, Environment and Technology (CIEMAT), Spain

Abstract - *This study continues the effort initiated in [1] [S. Smolentsev et. al., An Approach to Verification and Validation of MHD Codes for Fusion Applications, Fusion Eng. Des., 100, 65 (2015)] on verification and validation of computer codes for liquid metal flows in a magnetic field for fusion cooling/breeding applications. A group of experts in computational magnetohydrodynamics from several institutions in the US and Europe performed a code-to-code comparison for the selected reference case of a mixed-convection buoyancy-opposed magnetohydrodynamic flow of eutectic alloy PbLi in a thin-wall conducting square duct at Hartmann number Ha=220, Reynolds number Re=3040, and Grashof number Gr= 2.88×10^7. As shown, the reference flow demonstrates a boundary layer separation in the heated region and formation of a reversed flow zone. The results of the comparison suggest that all five solvers predict well the key flow features but have moderate quantitative differences, in particular, in the location of the separation point. Also, two of the codes are more computationally dissipative, showing no velocity and temperature oscillations.*

Keywords — *Liquid metal blanket, MHD flows, heat transfer, high-performance computations, code verification and validation.*

Note — *Some figures may be in color only in the electronic version.*

I. INTRODUCTION

Liquid metals (LMs) are promising working fluid candidates for blankets and plasma facing components (PFCs) of a fusion power reactor. When LM is circulating in a reactor for tritium breeding and/or cooling in the presence of a strong plasma-confining magnetic field, the LM flows experience strong magnetohydrodynamics (MHD) effects [2]. As widely recognized, full understanding and accurate prediction of MHD phenomena in LM flows and their impact on heat and mass transfer is critically important to the development of new LM concepts or improvement of the existing designs. However, despite several significant explorations in recent times, current knowledge in the area of MHD Thermofluids under specific fusion conditions is limited because of various simplifications under which prior studies were conducted. There is a dearth of comprehensive experimental and analytical studies of these flows when the key parameters (Hartmann *Ha*, Reynolds *Re*, and Grashof *Gr* numbers) vary over a wide range in complex flow and wall configurations as expected in the LM breeding/cooling applications [3]. Given that

*E-mail: sergey@fusion.ucla.edu

conditions of a fusion reactor cannot be fully reached in experiments, computer modeling of MHD flows coupled with heat and mass transfer is the only viable and effective design and analysis tool.

All present Computational Magnetohydrodynamics (CMHD) codes used for analyses of MHD flows with heat and mass transfer in fusion LM applications run into three major categories [1]. The first category is comprised of customized commercial multi-purpose CFD codes with a built-in or user-defined MHD module. Four typical examples of such codes are FLUENT (now a part of ANSYS), CFX (also a part of ANSYS), SC/TETRA by CRADLE and FLUIDYN by TRANSOFT International. Another code, which can be added to this group, is OpenFOAM, an open-source multi-purpose CFD toolbox with a built-in electromagnetic module developed by OpenCFD Ltd. COMSOL Multiphysics also provides an MHD capability that can be utilized either through the built-in physics modules or through the user-defined equation-based module.

The second category includes massive, non-commercial, "home-made" solvers, which are specially developed for MHD applications. Among such codes are HIMAG (USA) [4] and an MHD code called MTC (China) [5]. Unlike the commercial codes, these codes do not have a convenient user interface and typically need to be modified to meet specifications of a particular problem. This makes such codes less attractive to the potential users compared to the commercial codes. The advantages of such codes are, however, their focusing on MHD problems and flexibility compared to "black-box" commercial codes.

The third category is represented by research codes, which are typically limited to a special type of flows and/or relatively simple flow geometries. A few relevant examples are the research codes based on asymptotic techniques, which can be applied to inertialess flows, sometimes called the core-flow approximation [6], and the TRANSMAG code for analysis of MHD induced corrosion of ferritic steels in flowing lead-lithium alloy [7]. Many other examples of research codes can be found elsewhere. As a matter of fact, the most of the progress on blanket design & analysis and development of LM PFCs has been achieved so far using the research codes. A special group of research codes that address MHD turbulent flows includes Direct Numerical Simulation (DNS) [8] and Large Eddy Simulation (LES) [9] for simple geometries.

In spite of the significant recent progress in the development of computational tools under all three categories listed above, the field of CMHD is still not mature enough compared to its classical counterpart, CFD (Computational Fluid Dynamics). The limitations are related to the number of available codes, their applicability to real engineering problems, computational effectiveness, and even user confidence in the codes. To advance existing CMHD tools to the desired maturity level where associated physical/mathematical models and numerical codes provide a real predictive capability, a number of mandatory steps needs to be taken, including further code development and testing. Among them, verification and validation (V&V) is, perhaps, the most important step. A campaign on systematical V&V of MHD codes for LM blanket applications was initiated in [1], where a benchmark database of five problems was proposed to cover a wide range of MHD flows from laminar, fully developed to turbulent flows. In the present study, the database is extended to one more important class of buoyancy-driven MHD flows, which was underrepresented in [1]. The case of a buoyancy-opposed mixed-convection MHD flow in a conducting square duct was selected as a reference test case and then code-to-code comparisons were performed by an international team. The comparison has involved five existing CMHD codes: HIMAG, COMSOL, ANSYS FLUENT, ANSYS CFX, and OpenFOAM.

The selected comparison case belongs to the class of buoyancy-driven MHD flows where buoyancy forces are superimposed on the forced flow resulting in a mixed-convection flow regime. Buoyancy-induced flows in fusion blankets may have a characteristic velocity of 10-20 cm/s (depending on the considered blanket concept and on the orientation of blanket modules with respect to the gravity vector) and thus are important to all LM blanket concepts, which are presently under consideration. In a Dual Coolant Lead Lithium (DCLL) blanket, the eutectic lead-lithium (PbLi) alloy circulates for tritium breeding and cooling in long poloidal ducts at ~ 10 cm/s; the pressure-driven circulation flow velocity and that due to the buoyancy forces are of the same order [10]. The buoyancy effects are most important to Helium Cooled Lead Lithium (HCLL) [11] and Water Cooled Lead Lithium (WCLL) [12] blankets, where PbLi circulates at a very low velocity of the order of mm/s or less for tritium breeding, while He gas or water is used as a coolant. Even in a self-cooled PbLi blanket (SCLL) [13], where the PbLi velocity is significantly higher (~0.5-1 m/s) compared to other PbLi blankets, buoyancy effects cannot be neglected.

The topic of mixed-convection MHD flows in horizontal and vertical ducts has recently received considerable attention in literature from both computer modelers and experimentalists but the number of studies focusing on vertical flows is relatively small. Depending on the flow direction with respect to the gravity vector (upwards/buoyancy-assisted or downwards/buoyancy-opposed), heating scheme (surface or volumetric) and the wall electrical conductivity, the flow behavior in a vertical duct might be very different with regard to instabilities, transition to turbulence, dominance of 2D or 3D features, and formation of special flow patterns. Typical instabilities are known to be of the Kelvin-Helmholtz type and are usually attributed to inflection points in the velocity profile [14]. Recent experiments for mixed-convection vertical flows in a transverse magnetic field have shown significant low frequency, high magnitude temperature fluctuations in both circular pipe and rectangular duct flows heated from the wall [15-17]. Analytical solutions obtained in [18] for fully developed mixed-convection flows in a non-conducting duct with non-uniform, exponential volumetric heating suggest that locally reversed flows near the “hot wall” can be formed, providing that the main flow is downward and the Grashof number is high enough. Numerical computations based on the full 3D flow model [19] and the quasi-two-dimensional (Q2D) flow model [19- 21] also predict instabilities and flow reversals with a strong magnetic field effect. It should be noted that almost all 3D studies of mixed-convection MHD flows have demonstrated dominating Q2D flow dynamics, such that turbulent eddies are stretched in the direction of the applied magnetic field, exhibiting almost no variations along the magnetic field lines in the flow bulk.

The present paper is aimed at V&V of existing MHD codes for a particular class of mixed-convection MHD flows where the fluid flow and heat transfer are closely coupled due to buoyancy effects. First, we describe the reference mixed-convection flow case, introduce the comparison protocol and details of the codes and computational procedures, and then compare the most important results, including time-averaged and instantaneous velocity, temperature and electric potential distributions computed by the codes.

II. REFERENCE CASE

The reference case of a vertical downward flow in a square duct selected for the code-to-code comparison study (Fig. 1) resembles geometry of a DCLL blanket because of a long flow path

that, in principle, allows for a fully developed flow regime. In a real blanket, the poloidal flow length varies from ~ 2 m (modular blanket) [22] to a full "banana" segment of ~ 10 m [23], whereas in the reference case the vertical length is 2 m. The cross-sectional dimensions in the reference case are about 4 times smaller compared to a blanket: 5 cm by 5 cm, including a thin steel wall, $t_w = 2$ mm. Such dimensions were selected to fit the workspace of the electromagnet in the MaPLE facility [24]. As a matter of fact, all dimensions and other parameters in the reference case meet the specifications of the experimental MaPLE facility, such that a benchmarking experiment on a mixed-convection flow could be performed in the future. However, at the time of writing the paper, experimental data were not available.

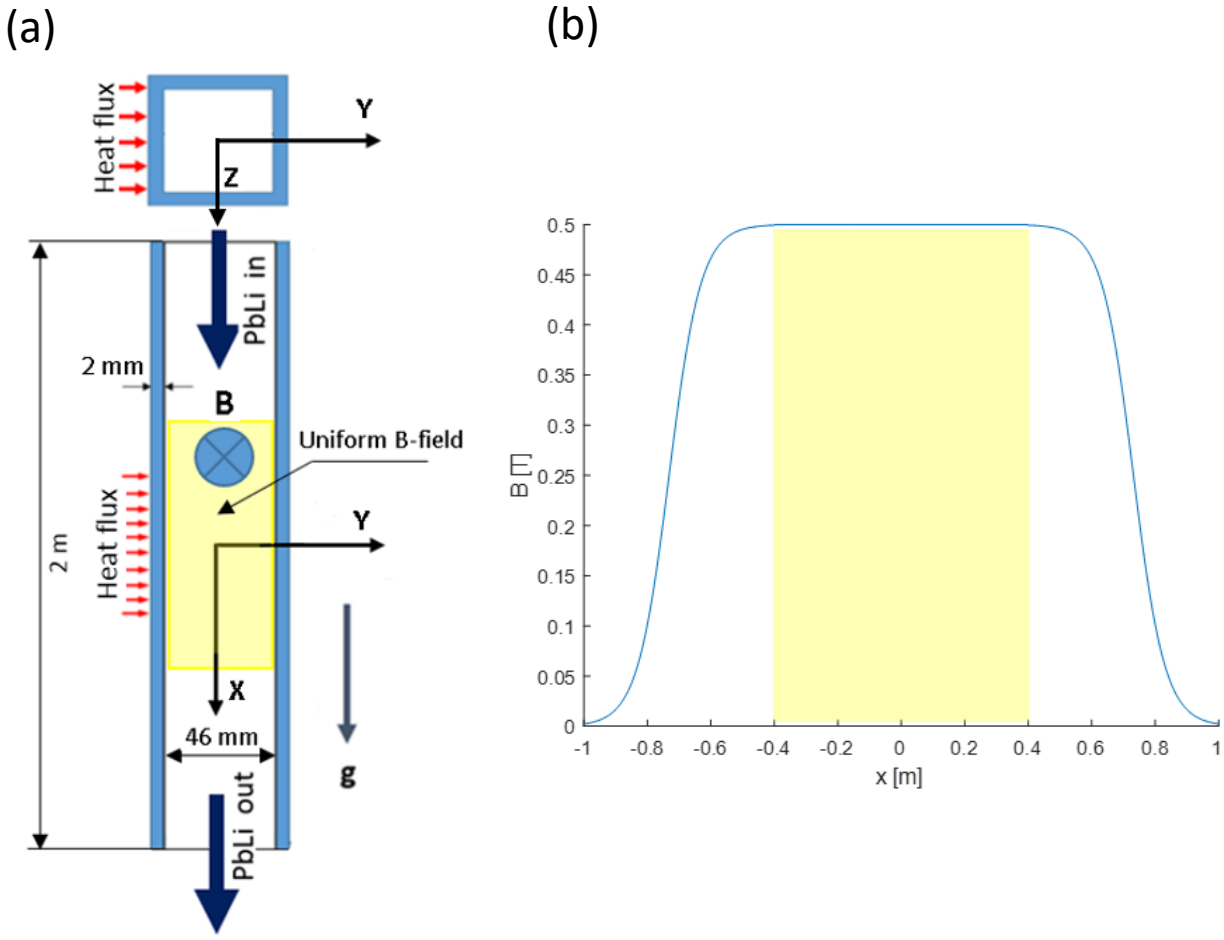

Fig. 1. Reference case of a downward mixed-convection MHD flow. (a) Sketch showing the PbLi flow carrying duct, flow direction, gravity vector, applied heat flux, uniform magnetic field region and coordinate axes, including top view and midplane. (b) Applied (transverse) magnetic field distribution.

In the reference case, PbLi, enters a vertical square duct from the top and flows downwards. One of the duct walls is uniformly heated over a distance of 0.6 m as shown in Fig. 1a. All other walls are thermally insulated. The flow is subjected to a transverse magnetic field, whose distribution along the axial coordinate is shown in Fig. 1b. The field distribution has two fringing

zones at the entry to and at the exit from the magnet, where the magnetic field varies from zero to a constant value. The uniform magnetic field length is ~ 0.8 m and the uniform field magnitude is B_0=0.5 T. In computations, the magnetic field was approximated with a formula that included a *tanh* function to reproduce both the uniform and fringing field regions. It should be noted that the heated section is 20 cm shorter than the uniform magnetic field length, while the entire duct is longer than the magnet such that the flow at the entry to and at the exit from the duct is purely hydrodynamic, without being affected by a magnetic field.

The thermophysical properties of PbLi and steel (SS 394) at the inlet temperature 300°C are shown in Table I. Other parameters used in the computations are the flow velocity U_0=0.03 m/s and the applied surface heat flux q''=0.04 MW/m^2. Using the dimensional data, the key dimensionless parameters can be computed as: $Ha = B_0 b\sqrt{\frac{\sigma_{PbLi}}{\nu\rho_{PbLi}}} = 220$, $Re = \frac{U_0 b}{\nu}$ =3040 and $Gr = \frac{g\beta b^4 q''}{\nu^2 k_{PbLi}}$ =2.88×10^7. All these parameters are constructed using the duct half-width b=0.023 m as a length scale. Another important dimensionless parameter (which is not directly used in the computations) is the wall conductance ratio $c = \frac{t_w\sigma_{ss}}{b\sigma_{PbLi}} = 0.12 \gg 1/Ha$, suggesting that a significant fraction of the electric current generated in the bulk flow closes its path through the electrically conducting wall.

Table I. Physical properties of PbLi and SS 394 at 300°C used in the computations.

Physical Property	**PbLi**	**SS 394**
Density ρ, kg/m^3	9486	7800
Kinematic viscosity ν, m^2/s	2.27×10^{-7}	
Electrical conductivity σ, S/m	7.89×10^5	1.09×10^6
Specific heat capacity C_p, J/kg-K	200.2	500.0
Thermal conductivity k, W/m-K	13.1	19.0
Volumetric expansion coefficient β, 1/K	1.774×10^{-4}	

III. CHARACTERIZATION OF THE FLOW

A description of the flow and temperature field is provided in this section based on recent studies of mixed convection flows in [25] using the HIMAG code. Figure 2 shows downstream variations of the velocity and temperature, including instantaneous and time-averaged fields. Uniform, isothermal flow of PbLi enters from the top (Fig. 2c, x=-0.99 m) and begins developing hydrodynamically as the LM moves downstream. Once the liquid enters the magnetic field zone, the flow starts experiencing MHD effects. The transverse applied magnetic field (**B$_0$**) interacts with the LM flow to produce circulations of electric current (**j**) and associated electromagnetic Lorentz forces (=**j**×**B$_0$**) that strongly affect the fluid's motion. Moving into the uniform magnetic field region, the still isothermal flow exhibits an M-shaped velocity profile (Fig. 2c, x=-0.46 m). Such flow is characterized by uniform velocity inside a central "core" or "bulk" region, very thin Hartmann boundary layers attached to the walls perpendicular to the magnetic field, and thin jets attached to the sidewalls, which run parallel to the magnetic field. The sidewall jets are a consequence of rotational (curl(**j**)≠0) electric currents closing through the electrically conducting

walls. At the beginning of the heated region, a thermal boundary layer starts to develop on the heated wall as heat propagates into the LM flow. The "warm" fluid experiences a buoyant force in the direction opposite gravity, which, in this case, is opposite the flow direction. On startup, the temperature increases slowly as the LM moves downwards along the heated wall, and, as the flow there becomes increasingly buoyant, the velocity near the heated wall diminishes, resulting in an asymmetric velocity profile (Fig. 2c, x=-0.20 m). Further downstream, once the buoyant force exceeds the pressure gradient, the flow near the heated wall stagnates and then reverses to generate sufficient viscous and electromagnetic forces to balance the buoyancy. A recirculating flow profile forms, with "hot" fluid moving upwards attached to the hot wall and "cold" fluid moving downwards at the opposite wall (Fig. 2c, x=0.07 m). The characteristic flow patterns that form in the transition from the M-shaped velocity profile to the reversed flow are the separation of the boundary layer that occurs at a short distance downstream from the beginning of the heated region (Fig. 3a) and the "*reversed flow bubble*" that can be seen near the heated wall stretching over about half of the length of the heated zone (Fig. 3b). Figure 3b also shows the important effect of Joule dissipation that results in smoothening the velocity field and dampening fluctuations along the magnetic field direction such that the streamlines are mostly confined to the planes perpendicular to the magnetic field (xz-planes).

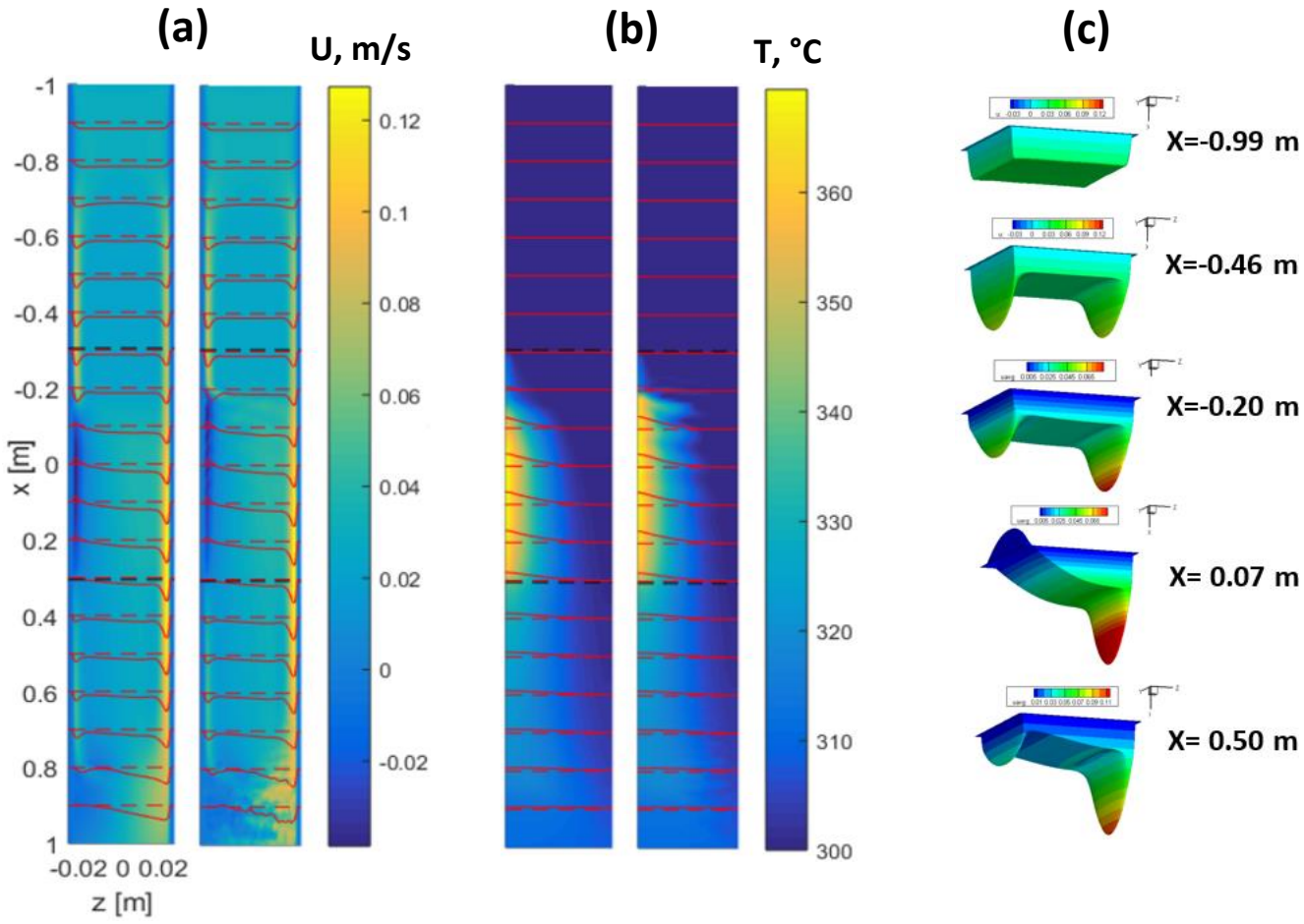

Fig. 2. Velocity and temperature distributions computed with HIMAG. (a) Time-averaged (left) and instantaneous (right) axial velocity component in the midplane. (b) Time-averaged (left) and instantaneous (right) temperature in the midplane. (c) Time-averaged velocity profiles at five axial locations.

The dominating Q2D flow behavior is changed near the boundary layer separation point at the beginning of the reversed flow bubble where the flow does exhibit some 3D features (Fig. 3b). As seen from Figs. 2 and 3, inside the heated zone, the flow becomes about fully developed between x=-0.1 m and x=0.2 m, which is about the half of the heated length. At the end of the heated region, the boundary layer reattaches to the heated wall and the flow slowly begins to redevelop towards the M-shaped velocity profile (Fig. 2c, x=0.50 m). Among other interesting peculiarities observed in the HIMAG computations is the unsteady flow behavior as seen in Fig. 2 and also in Fig. 4. As computed by HIMAG, the velocity fluctuations are about 15% of the circulation velocity and the temperature fluctuations are about 5% of the inlet value.

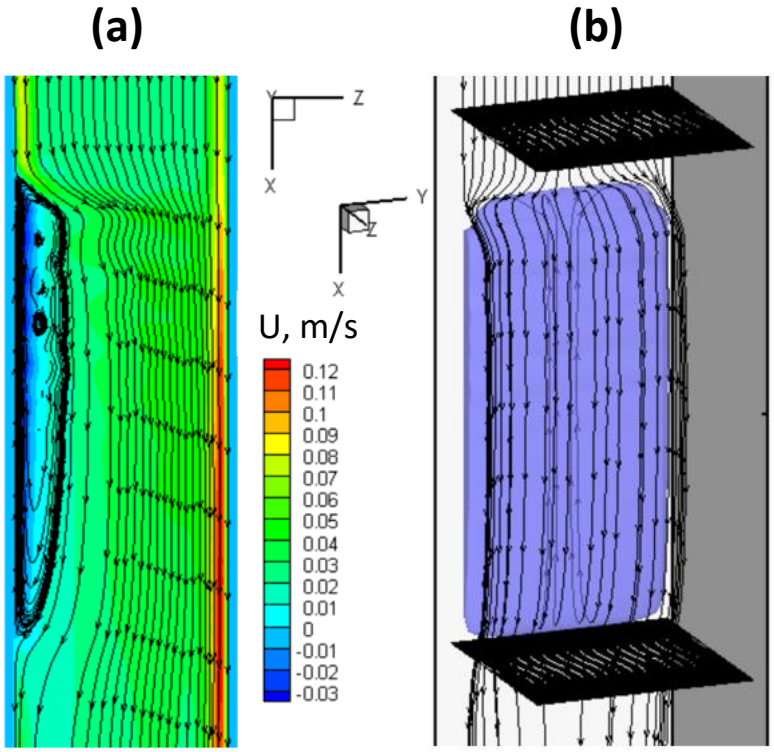

Fig. 3. Special features of the reference mixed-convection flow. (a) Separation and reattachment of the boundary layer on the heated wall. (b) Formation of a reversed flow bubble.

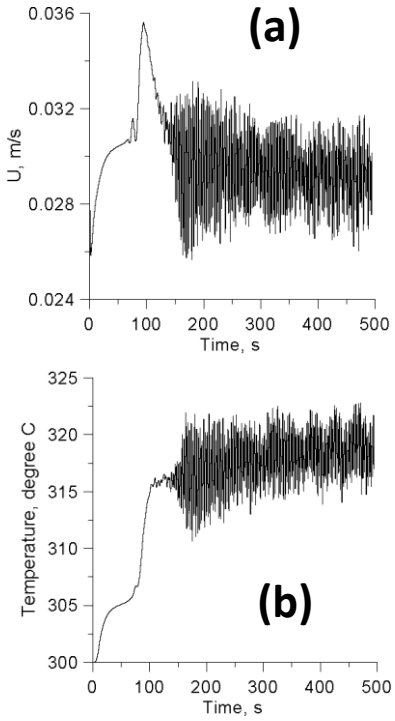

Fig. 4. Velocity (a) and temperature (b) fluctuations in the reference flow at x=0, y=0.00575 m, z=-0.00575 m.

IV. COMPARISON PROTOCOL

A number of requirements, rules, and procedures (hereinafter called "comparison protocol") were agreed upon by the code testers to regulate the computations, data output, and comparison of the computed results themselves. Among the mandatory requirements are the use of the same mathematical model, geometry, magnetic field distribution, heating scheme, and thermophysical properties as described in Section 3. As for the mathematical model, the 3D Navier-Stokes equations for a flow of viscous, incompressible fluid coupled with electromagnetic equations and the energy equation are used. The electromagnetic part of the model is based on the induced

electric potential. The buoyancy effects are included in the model using the Boussinesq approximation in which density differences are ignored except where they appear in the buoyancy force term on the right-hand-side of the momentum equation. These governing equations are shown below:

$$\nabla \cdot \mathbf{U} = 0, \tag{1}$$

$$\frac{\partial \mathrm{U}}{\partial t} + \mathbf{U} \cdot \nabla \mathbf{U} = -\frac{1}{\rho}\nabla p + \nabla \cdot \nu \nabla \mathbf{U} + \frac{1}{\rho}\mathbf{j} \times \mathbf{B_0} - \mathbf{g}\beta(T - T_o), \tag{2}$$

$$\mathbf{j} = \sigma(-\nabla \phi + \mathbf{U} \times \mathbf{B}_0), \tag{3}$$

$$\nabla \cdot \mathbf{j} = 0, \tag{4}$$

$$\rho c_p \left(\frac{\partial T}{\partial t} + \mathbf{U} \cdot \nabla T\right) = \nabla \cdot k \nabla T. \tag{5}$$

In the above equations, **U** is the velocity vector, T is the temperature, **j** is the electric current density vector, ϕ is the electric potential, $\mathbf{B}_0$ is the applied magnetic field and T_0 is the temperature at the flow inlet. Other parameters are explained in Section 3. The MHD flow equations are written here in the so-called inductionless approximation, where the induced magnetic field is neglected compared to the applied one. The equation for Ohm's law (3) and the continuity equation for the induced electric current (4) can be combined in one equation for the electric potential:

$$\nabla \cdot (\sigma \nabla \phi) = \nabla \cdot (\sigma \mathbf{U} \times \mathbf{B_0}). \tag{6}$$

All codes used in the comparison solve Eqs. (1-6) but in a different way. The numerical procedures used by each code are explained in Section 5. The mandatory boundary conditions are no slip velocity at the duct walls, constant heat flux within the heated region, ideal thermal insulation for other non-heated walls, and zero wall-normal current component on all outer wall surfaces. Regarding the inlet/outlet boundary conditions, each team made their selection of several possible variants ensuring a mean entrance flow velocity of 0.3 m/s and the inlet temperature of 300°C. Also, each team was responsible for the computational mesh, selection of a particular solver and computational settings, and testing the code, including mesh sensitivity studies. It was suggested to perform as much testing as needed to make sure that the MHD flow in the reference case would be adequately resolved. Although not all five tests recommended in [1] were finished by the teams, all codes were successfully tested against the Hunt and Shercliff solutions at high Hartmann numbers of the order of 10^4.

Special attention was paid to the data output and presentation of the results in the same format such that the results could be plotted with the same graphical tool and then directly compared. Each team was responsible for the data conversion and sharing the data files with others of the following results:

- 2D time-averaged velocity and temperature distribution in the duct midplane z=0;
- 1D time-averaged velocity and temperature distributions as a function of z (between the side walls) at five axial positions within the heated zone x=-0.15, -0.05, 0.05, 0.15 and 0.25 m at y=0;
- Time-averaged temperature along the duct axis (at y=0, z=0);

- Time-averaged mean bulk temperature as a function of x;
- Time-averaged induced voltage between two side walls at y=0;
- Time-averaged wall shear stress as a function of x at y=-0.023 m and z=0;
- Fluctuating velocity [$U(t)$,V(t),W(t)] and temperature $T(t)$ at the center of the duct (x=y=z=0).

Such data selection allows for the full characterization of the key flow features, including the flow reversal, separation of the boundary layer from the wall inside the heated region and its reattachment downstream, and unsteady flow behavior. On the other hand, these data provide a good basis for the comparison to demonstrate to what degree each code captures the flow and to reveal differences in the computed results among the codes.

V. CODES AND COMPUTATIONAL PROCEDURES

This section introduces the most important computational details for each of the five codes.

HIMAG. HIMAG is a 3D MHD finite-volume solver developed by HyPerComp Inc. and UCLA [4]. The first 200 000 time-steps used upwind scheme. Otherwise, the computations employed second order central-symmetry approximation of the convective terms in the momentum and energy equations to avoid unwanted flow damping caused by the schematic viscosity. Simulations were run in parallel using 1024 cores on CORI and EDISON super computers at National Energy Research Scientific Computing Center (NERSC). The computations were conducted over a 500-second time interval, sufficient to reach a statistically steady-state flow and then to perform time-averaging. This requires about 3 full days to complete. Time-step size is 1×10^{-4} s for high temporal resolution and to assure stable computations. High viscosity 40 cm region was added at the end of the original 2-meter section to damp artificial flow oscillations that were observed in the first computations, possibly due to reflections of the vortices from the outlet boundary. The inlet boundary conditions assure uniform velocity profile, uniform inlet temperature, zero axial current and zero pressure gradient. The outlet boundary conditions include zero velocity gradient, zero temperature gradient, no axial currents and zero pressure. Three non-uniform meshes (with clustering nodes within the Hartmann and side layers) were employed in the test computations: coarse (188, 64, 65), medium (236, 80, 80), and fine (297,100,100). As almost no differences were observed between the medium and the fine mesh, the final computation was run using the medium mesh with the total number of nodes of ~ 1.5×10^{6} that included 8 nodes in the Hartmann layers and 10 nodes inside each side layer. Time averaging was performed over the interval from t_1=100 to t_2=490 s.

COMSOL. COMSOL MULTIPHYSICS is a cross-platform finite element analysis solver and multiphysics simulation software developed by COMSOL Inc. [26]. It allows conventional, physics-based user interfaces and coupled systems of partial differential equations. The computational set-up for the reference case involves three COMSOL modules: fluid flow, heat transfer, and electromagnetics. The system of spatially discretized equations in each module is linearized with the Newton-Raphson method. The linearized equations for the velocity and pressure are then solved simultaneously with a direct solver (Pardiso), while the other two for the temperature and electric potential are solved using an iterative conjugate gradient method. Time marching is performed at a time-step of 0.05 s. The computational time interval is 470 s. The computations were run using a 2 CPU DELL workstation (total number of computer nodes is 20), which allowed for 300 time-steps per day. Taking into account symmetry with respect to the y=0

plane, only half of the domain was computed. The entire computation took about one month. Similar to HIMAG, 3 different meshes were tested in the preliminary mesh sensitivity study: "normal", "fine", and "finer". The final computation for the reference flow was performed using the normal mesh that included 200 elements in the flow direction and 48 by 48 elements in the cross-sectional plane resulting in 461×10^3 elements total. This mesh provided 6 elements in the Hartmann and 8 elements in the side layers.

ANSYS FLUENT. ANSYS FLUENT uses a finite-volume method [27]. A pressure-based solver was employed that includes second order approximations for the pressure gradient and a second order upwind scheme for the convective terms in the energy and momentum equations. The upwind scheme requires cell centered values for each cell and cell centered gradients in the upstream cell. In FLUENT, Green-Gauss node based scheme is used for gradient evaluation. The time marching is based on the second-order time-discretization scheme with a constant time increment of 0.01 s. The mesh size was similar to the "medium" mesh in the computations by HIMAG, i.e. 236×80×80. A hyperbolic function based coordinate transformation was applied to cluster the nodes inside the boundary layers. There were at least 10 nodes inside each boundary layer. Mesh sensitivity studies were not performed. The time interval is 747 s of which a 600-second sub-interval was used for averaging results in time. The entire computation took 20 days using a single CPU 16-core workstation.

ANSYS CFX. The computations utilized the CFX transient solution algorithm [28], assuming a laminar flow regime. The code adopts a finite-volume method. Pressure-velocity coupling is enforced via simultaneous solution of a linearized system of algebraic equations obtained from the momentum and mass conservation equations. The linearized equations are solved iteratively using a multigrid solver accelerated by the use of the incomplete factorization technique. Time marching is performed using the second order backward Euler scheme. To compute the convective terms, a first order upwind scheme is used first over the time interval of 260 s and then changed to a more robust second-order high-resolution scheme, which has a numerical advection correction term to partially compensate the numerical diffusion inherent to the lower order upwind schemes. The total time interval is 1030 s, including the time-averaging interval in the final phase of the computations from t_1=550 s to t_2=1030 s. The entire computation took approximately three weeks using 24 cores (Xeon E5-2690, 2.6 GHz) on the HORUS cluster at Sapienza University. The initial time-step of 10^{-6} s was gradually increased to 0.015 s at t=20 s and then kept unchanged. Similar to other codes, the mesh sensitivity study was performed first. In this study, 3 non-uniform meshes (coarse, medium and fine) were tested for a simpler isothermal MHD flow problem. Eventually, the fine mesh of about 2.2×10^6 nodes, including 200 uniformly distributed nodes in the axial direction over the 2-meter duct and 72×154 clustered nodes within a duct cross-section was selected for further computations. Of these nodes, 8 nodes were placed inside each Hartmann layer, 8 in the wall, and 30 inside the side layer.

OpenFOAM Equations (1-6) have been implemented in the open source software OpenFOAM [29]. The solver is based on a finite-volume method and uses a co-located grid, *i.e.* the fluid dynamic variables are stored at the centroid of the control volume. The Pressure Implicit with Splitting of Operators (PISO) algorithm is used for pressure-velocity coupling to satisfy mass conservation. The pressure equation is solved by a preconditioned conjugate gradient (PCG) method and the velocity equation by a PBiCG algorithm. For solving electric potential and temperature equations, a PBiCG method with diagonal-based incomplete Cholesky preconditioner was selected. The time marching is performed using the second order backward Euler scheme. A second order accurate discretization scheme is used for the convective terms. Three grids have

been used to perform a grid sensitivity study. The final mesh used for the simulation is characterized by 80×80 points in the duct cross-section, with 7 nodes in the Hartmann layer and 25 nodes in the parallel layers. There were 530 nodes in the axial direction distributed over a length of 3 m. This results in a total number of 4.39×10^6 grid points. Simulations are run in parallel using 710 processors on Marconi HPC in Italy. The computations were conducted over a time interval of 550 s, with an initial time step of 10^{-4} s, which was increased up to 10^{-3} s. About 5 days are necessary to complete the simulation for the highest spatial resolution. As hydrodynamic entrance conditions far upstream of the magnetic field region, zero axial gradient for pressure, uniform velocity of 0.03 m/s, zero electric potential and inlet temperature of 300°C were imposed. At the outlet, far downstream of the magnet, hydrodynamic conditions of zero pressure and zero electric potential were used while the velocity and temperature were assumed to have zero axial gradient.

VI. COMPARISON OF THE COMPUTED RESULTS

Figure 5 shows the temperature and Fig. 6 the velocity distribution in the duct midplane. Both figures clearly demonstrate the most interesting features of the mixed-convection buoyancy-opposed MHD flow, namely: development of the boundary layers, formation of the near-wall jets in the inlet section upstream of the heated zone, separation of the boundary layer from the heated wall and its reattachment downstream, and formation of the reversed flow. The details are, however, different among the codes. One can see that the axial location of the boundary layer separation point and that of the flow reattachment are different. Also, velocity and temperature distributions in the outlet section downstream of the heated zone are not exactly the same. This means that all the codes capture well the most important flow physics but there are quantitative differences.

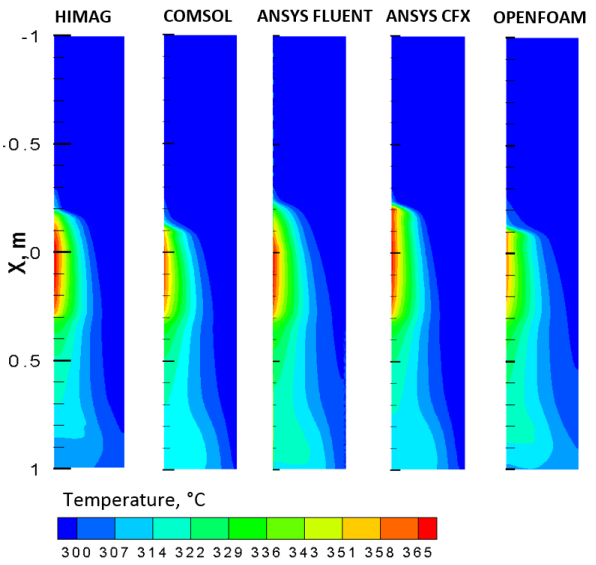

Fig. 5. Time averaged temperature in the duct midplane y=0.

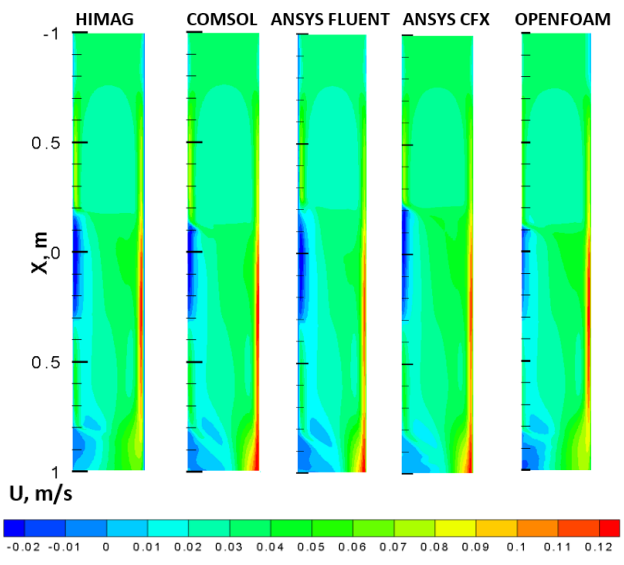

Fig. 6. Time averaged velocity (*U*) in the duct midplane y=0.

Such discrepancies are further seen in Figs. 7 and 8 showing time averaged 1D temperature and velocity distributions. The most significant differences are observed at the first measuring station at x=-0.15 m. Here, of the five codes, COMSOL shows the lowest wall temperature on the heated wall and a velocity profile still resembling the M-shaped profile but with a lower velocity peak near the heated wall, while other codes demonstrate a reversed flow velocity profile.

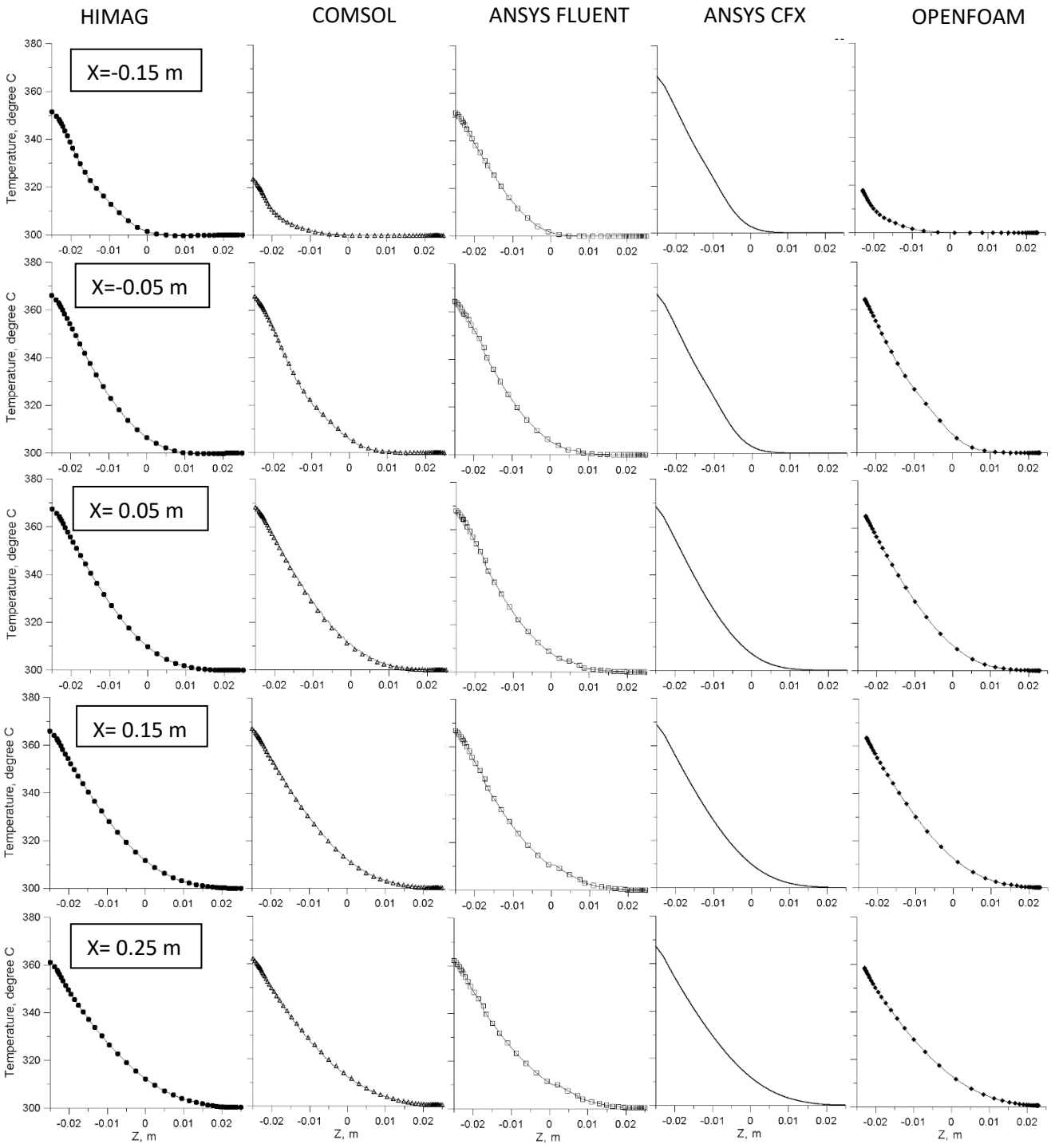

Fig. 7. Time-averaged temperature at five locations along the heated section length.

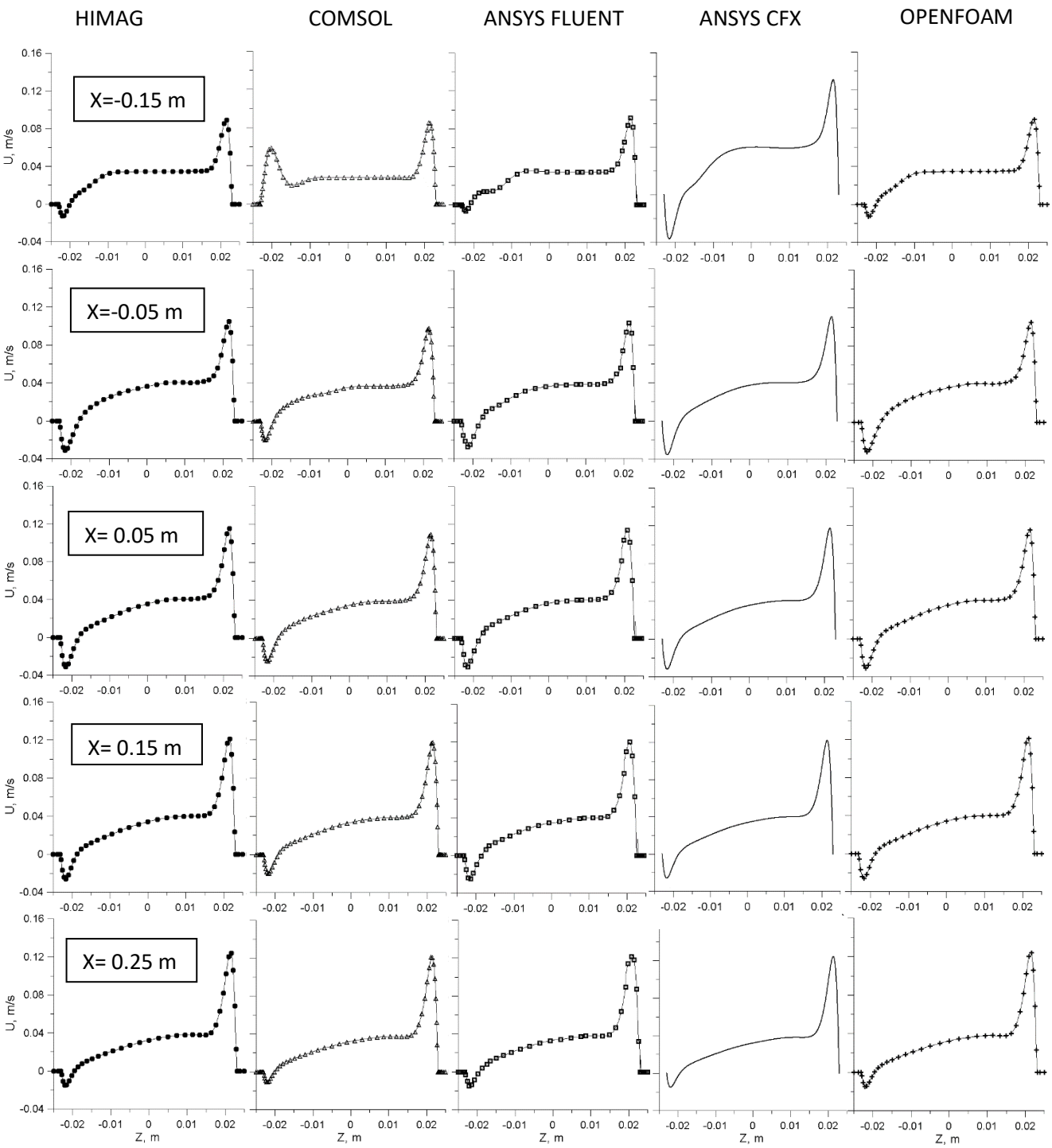

Fig 8. Time-averaged velocity (U) at five locations along the heated section length.

Downstream of the second measurement station at x=-0.05 m (i.e. almost near the center of the heated zone), all codes demonstrate very similar temperature and velocity distributions. Moreover, within the length from *x*=-0.05 to *x*=0.15 m, all the codes predict a fully developed flow as there are no visible variations in the velocity field, as seen in Fig. 8. In this fully developed flow, the

velocity profile is extremely asymmetric with the minimum negative velocity of about -0.035 m/s near the heated wall and about 0.12 m/s near the opposite wall.

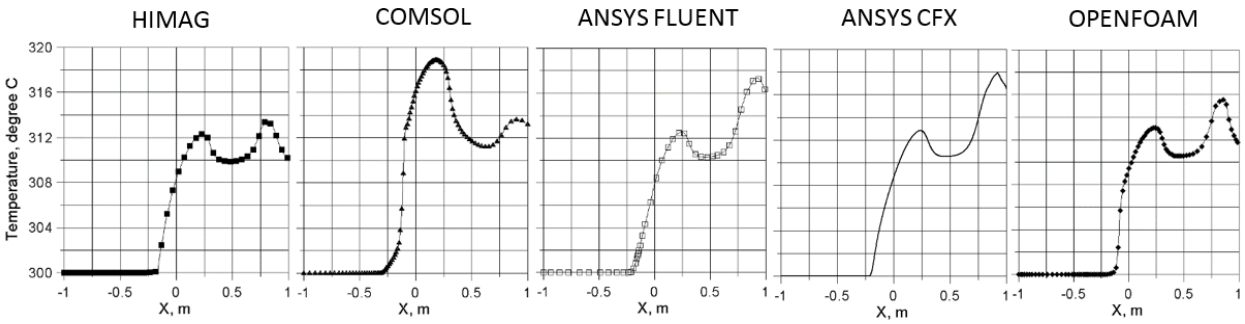

Fig. 9. Time-averaged temperature at the duct axis.

Significant discrepancies can be seen in Fig. 9 that shows a time-averaged temperature at the duct axis. Although all codes predict monotonic temperature increase first and then non-monotonic behavior with two local peaks near $x \approx 0.15$ and $x \approx 0.9$ m, the peak temperatures are different. In fact, the two temperature curves computed by ANSYS FLUENT and ANSYS CFX are very close but different from other three codes. The highest temperature of ~ 319°C was demonstrated by COMSOL at the first peak. COMSOL also shows higher temperature at the first peak and lower temperature at the second peak, while other codes demonstrate an opposite trend. These variations in the temperature with the axial coordinate are related to significant changes in the velocity field when the flow develops downstream, first experiencing buoyancy forces within the heated zone and then being affected by strong electromagnetic forces associated with the axial currents in the fringing magnetic field zone.

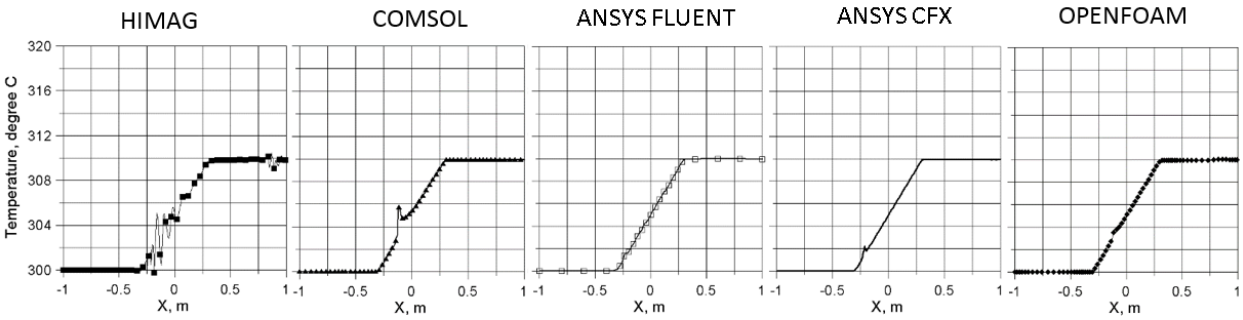

Fig. 10. Time-averaged mean bulk temperature. Note: HIMAG hasn't provided time-averaged data; instantaneous mean bulk temperature is shown instead.

Time-averaged mean-bulk temperature is shown in Fig. 10. This particular data set can be used for checking the energy conservation in each computation. Namely, the computed temperature difference ΔT between the flow inlet and outlet should match a simple analytical prediction based on the energy balance in the flow:

$$q'' S_q = \rho U_0 4b^2 C_p \Delta T. \quad (7)$$

Here, S_q is the area of the heated section and ρ and C_p are the PbLi density and specific heat capacity specified in Table I. From this formula, ΔT=9.95 K. As seen from Fig. 10, all five codes predict the same ΔT that matches very well the temperature difference from the formula. It is interesting that two codes, COMSOL and ANSYS CFX, show a local peak in the mean bulk temperature near the boundary layer separation point. A small distortion from the linear behavior is also seen at the same location in the OpenFOAM results.

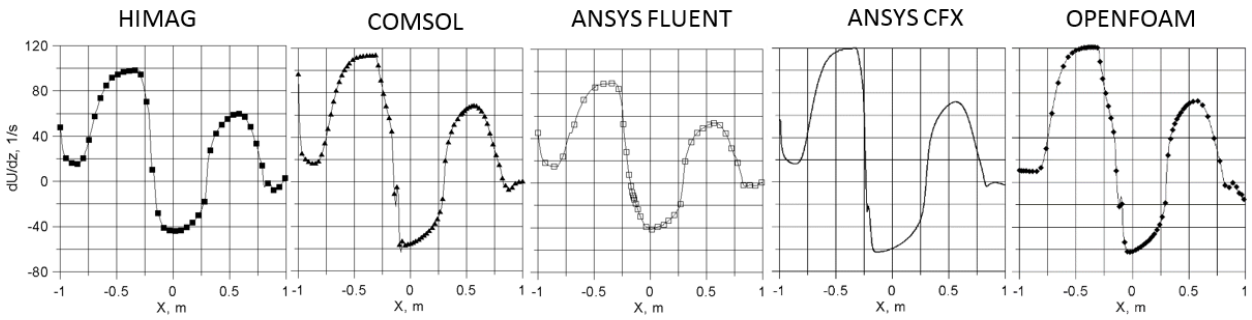

Fig. 11. Time-averaged wall shear stress at y=-0.023 m, z=0.

As was mentioned earlier, the codes have some discrepancy in predicting the location of the boundary layer separation point as seen, for example, in Fig. 6. To directly demonstrate the differences, a time-averaged velocity gradient dU/dz on the heated wall was plotted in Fig. 11 as a function of the axial coordinate. The condition dU/dz=0 indicates the boundary layer separation point. Table II summarizes the location of the separation point x_s computed with all codes.

Table II. Location of the boundary layer separation point on the heated wall computed with the codes.

Code	**HIMAG**	**COMSOL**	**ANSYS FLUENT**	**ANSYS CFX**	**OpenFOAM**
x_s, m	-0.17	-0.15	-0.18	-0.24	-0.14

As seen from the table, the separation occurs at some distance downstream from the leading edge of the heated section. However, the predictions of x_s differ significantly from -0.14 m (OpenFOAM) to -0.24 m (ANSYS CFX). The differences are significantly higher than the axial dimension of the computational cell in each computation and thus cannot be simply explained by a different mesh size.

An important computational aspect is the ability of a code to correctly reproduce time-dependent behavior of the flow. Most of the LM MHD flows in a breeding blanket are expected to be time-dependent, demonstrating Q2D turbulence [30]. Also, in the experimental conditions, the buoyant flows typically exhibit fluctuations [15-17]. As reported earlier in this paper, the HIMAG code has predicted significant velocity and temperature pulsations. COMSOL and OpenFOAM also predict fluctuations as seen in Fig. 12 for the velocity field and in Fig. 13 for the temperature field. The two other codes, ANSYS FLUENT and ANSYS CFX, have not demonstrated any fluctuations. Looking at the velocity pulsations in Fig. 12, one can conclude that turbulence appears in the special form of Q2D turbulence as the pulsating velocity component in the direction of the applied magnetic field (V) is two orders of magnitude lower than the axial

velocity pulsations (*U*) and at least one order of magnitude lower compared to the cross velocity pulsations (*W*). It should be noted that even though COMSOL computations do confirm the fluctuating nature of the flow, no fluctuations are seen in Fig. 12 for the *V* velocity component. This, however is a consequence of the symmetry boundary conditions used in the COMSOL computations at the duct midplane *y*=0 to reduce the computational domain to the half-size.

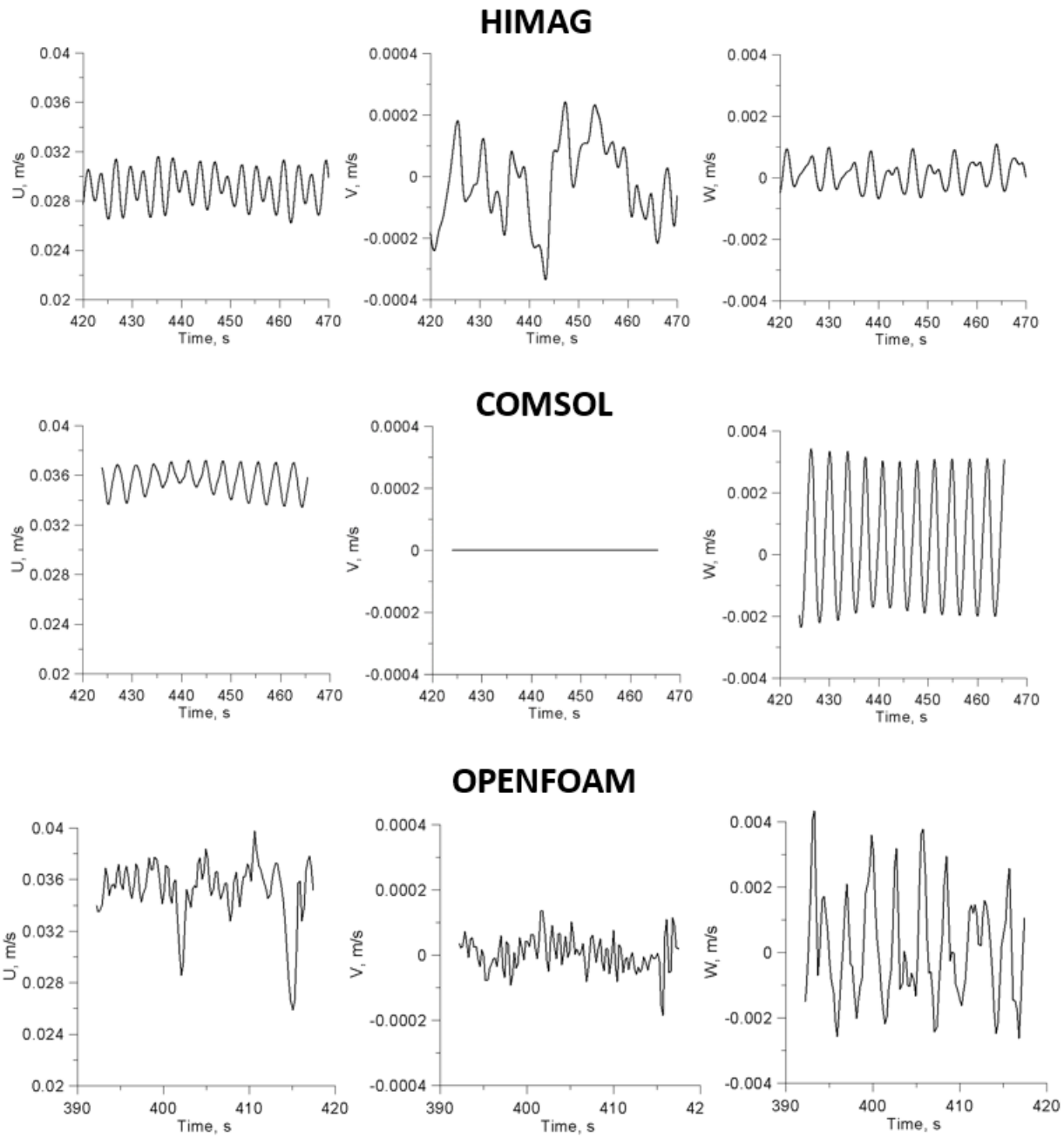

Fig. 12. Fluctuating velocity (*U*,*V*,*W*). COMSOL data at: *x*=0, *y*=0, *z*=0. HIMAG data at: *x*=0, *y*=0.00575 m, *z*=-0.00575 m. OpenFOAM data: *x*=0, *y*=0, *z*=0. ANSYS CFX and ANSYS FLUENT have shown no fluctuations in time.

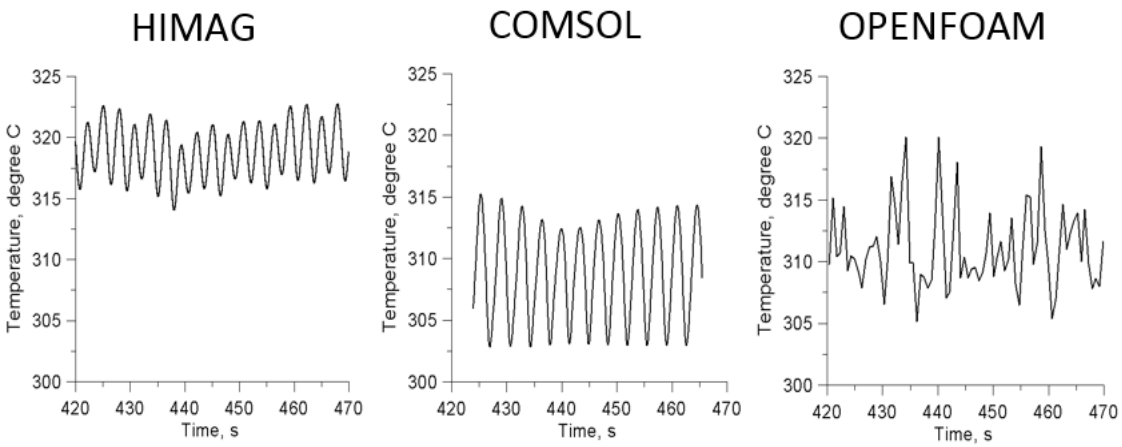

Fig. 13. Fluctuating temperature. COMSOL data at: x=0, y=0, z=0. HIMAG data at: x=0, y=0.00575 m, z=-0.00575 m. OpenFOAM data: x=0, y=0, z=0. ANSYS CFX and ANSYS FLUENT have shown no fluctuations in time.

The velocity and temperature fluctuations shown in Figs. 12 and 13 can also be used to estimate the characteristic frequency. Low frequencies are dominating in all computations that were able to resolve the fluctuating behavior at about 0.3 Hz. Although the three codes have demonstrated similar amplitude and frequency characteristics, the time-dependent behavior is obviously not the same. COMSOL has demonstrated near-harmonic fluctuations, whereas results computed by HIMAG and especially by OpenFOAM are more irregular. In part, that might be related to different locations of the monitoring point in the computations.

Obviously, the two ANSYS codes are too dissipative; that might be related to the use of upwind schemes by both codes. Even though both codes used a second order upwind scheme where the schematic viscosity is partially compensated, the codes were not able to reproduce the fluctuations unlike HIMAG, COMSOL and OpenFOAM. The absence of oscillations in the computations by the two ANSYS codes is also seen in Fig. 14 for instantaneous temperature.

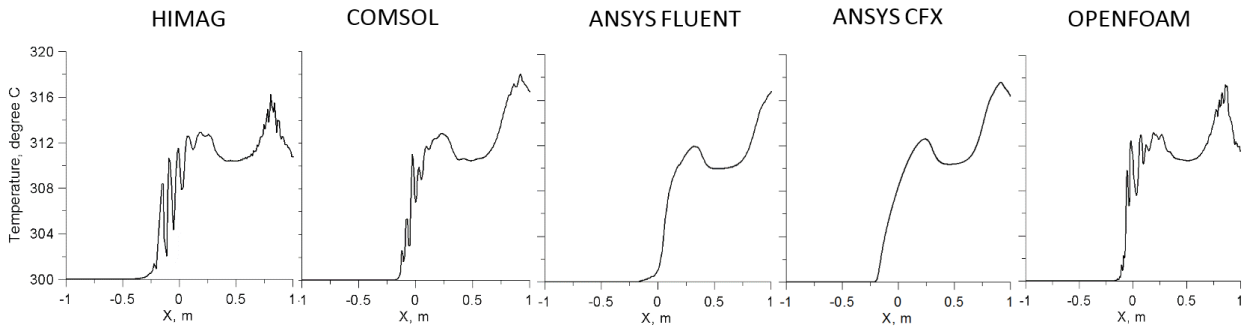

Fig. 14. Instantaneous PbLi temperature along the duct axis (y=0, z=0).

In Fig. 15, comparisons are performed for the induced voltage between the two side walls. A simple estimate based on the Ohm's law, suggests that without buoyancy effects at the flow velocity 0.03 m/s and 0.5 T magnetic field, the induced voltage in the PbLi flow would be tens of

millivolts. The computations directly confirm this estimate: all codes predict the maximum voltage of about 60 mV.

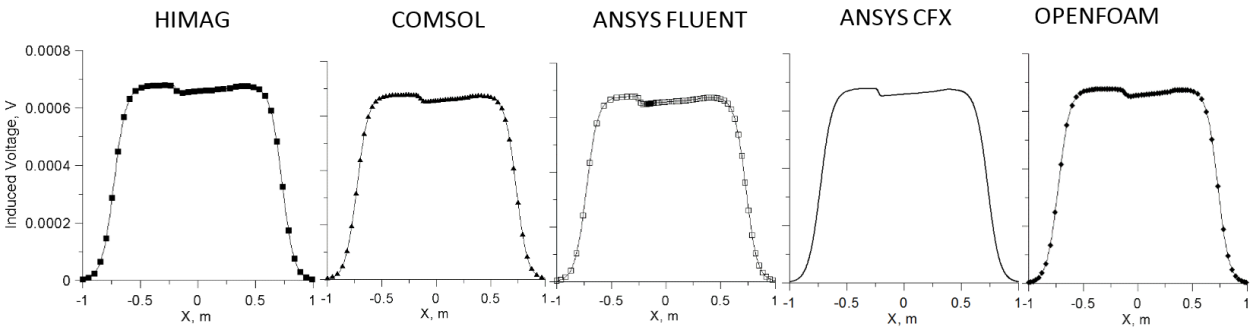

Fig. 15. Time-averaged induced voltage between two side walls along the centerline (y=0). Note: HIMAG hasn't provided time-averaged data; instantaneous voltage is shown instead.

Interestingly, in spite of all the discrepancies observed in the velocity and temperature distributions, the electric potential distributions computed by all five codes are very close. This is, however, not surprising because a similar trend was observed in other computations of MHD flows, for example in [31]. A small distortion in the distribution of the induced voltage at about the same location that corresponds to the separation point is clearly seen in all five computations. This suggests a simple, indirect approach for evaluation of the boundary layer separation point in experiments, because measuring the electric potential on the duct wall is much simpler compared to more delicate diagnostics for PbLi temperature and velocity field.

VII. CONCLUSIONS

Code-to-code comparisons have been perfomed for an MHD mixed-convection bouyancy-opposed flow at Ha=220, Re=3040, and Gr= 2.88×10^7 using five different solvers: HIMAG, COMSOL, ANSYS FLUENT, ANSYS CFX, and OpenFOAM. Most of the predictions for the time-averaged flow and heat transfer are very close among the codes. The most significant differences have been observed for the location of the boundary layer separation point that varied from code to code from -0.14 m to -0.24 m, which corresponds to about 4 characteristic lengths. Three codes, HIMAG, COMSOL, and OpenFOAM predicted pronaunced velocity and temperature fluctuations. The two ANSYS codes, FLUENT and CFX, were not able to reproduce the time-dependent flow behaviour, probably because of the high schematic viscosity associated with the use of the second order upwind scheme. In spite of the observed differences, the authors have agreed that this code-to-code comparison suggests that all codes are capable of resolving the most important flow features, such as boundary layer separation, reattachement and formation of a reversed flow. Therefore, these codes can be reccommended for their use for predicting LM MHD flow behaviour and heat and mass transfer in fusion cooling applications where electromagnetic and bouyancy forces are dominant. However, a special care should be taken to accurately resolve the unsteady flow features, including instabilities and Q2D turbulence. Such flow regimes are likely to happen in all LM blankets and in certain situations can be critical to the blanket functionality and performance.

As a final comment, it should be noted that the present comparison was performed for a relatively small magnetic field of 0.5 T (*Ha*=220) and for a small duct size compared to a blanket. In real fusion applications, the magnetic field (and the Hartmann number) is at least one order of magnitude higher. The duct cross-sectional dimension and the heat load in the blanket are also significantly higher, resulting in the Grashof number several orders of magnitude higher compared to the reference case in the present analysis. It remains to be proven that under such conditions the agreement would be of the same good quality.

Acknowledgemts

The UCLA team (TR, YY, and SS) aknowledges financial support from the DOE grant DE-FG02-86ER52123 and from the subcontract from the Oak Ridge National Laboratory #4000171188. Part of this work has been carried out within the framework of the EUROfusion Cosnsortium and received funding from Euratom research and training programme 2014-2018 and 2019-220 under grant agreement No 633053. The views and opinions expressed herein do not necessarily reflect those of the European Comission.

References

1. S. SMOLENTSEV et al., "An Approach to Verification and Validation of MHD Codes for Fusion Applications," *Fusion Eng. Des*., **100**, 65 (2015).

2. S. SMOLENTSEV, R. MOREAU, L. BÜHLER, C. MISTRANGELO, "MHD Thermofluid Issues of Liquid-metal Blankets: Phenomena and Advances, *Fusion Eng. Des*., **85**, 1196 (2010).

3. L. BÜHLER et al., "Facilities, Testing Program and Modeling Needs for Studying Liquid Metal Magnetohydrodynamic Flows in Fusion Blankets," *Fusion Eng. Des*., **100**, 55 (2015).

4. P. HUANG et al., "A Comprehensive High Performance Predictive Tool for Fusion Liquid Metal Hydromagnetics," HyPerComp Inc. (USA), Technical Report HPC-DOE-P2SBIR-FINAL-2017, 2017.

5. T. ZHOU, Z. YANG, M. NI, H. CHEN, "Code Development and Validation for Analyzing Liquid Metal MHD Flow in Rectangular Ducts," *Fusion Eng. Des*., **85**, 1736 (2010).

6. L. BÜHLER, "Magnetohydrodynamic Flows in Arbitrary Geometries in Strong, Nonuniform Magnetic Fields - A Numerical Code for the Design of Fusion Reactor Blankets," *Fusion Tech*., **27**, 3 (1995).

7. S. SMOLENTSEV, S. SAEIDI, S. MALANG, M. ABDOU, "Numerical Study of Corrosion of Ferritic/Martensitic Steels in the Flowing PbLi with and without a Magnetic Field," *J. Nuclear Materials*, **432,** 294 (2013).

8. D. KRASNOV, O. ZIKANOV, T. BOECK, "Numerical Study of Magnetohydrodynamic Duct Flow at High Reynolds and Hartmann Numbers," *J. Fluid Mech*., **704**, 421 (2012).

9. H. KOBAYASHI, "Large Eddy Simulation of Magnetohydrodynamic Turbulent Duct Flows," *Phys. Fluids*, **20**, 015102 (2008).

10. S. SMOLENTSEV, N.B. MORLEY, M. ABDOU, S. MALANG, "Dual-Coolant Lead-Lithium (DCLL) Blanket Status and R&D Needs," *Fusion Eng. Des*., **100**, 44 (2015).

11. G. RAMPAL et al., "HCLL TBM for ITER-Design Studies," *Fusion Eng. Des*., **75-79**, 917 (2005).

12. L. GIANCARLI et al., "Water-Cooled Lithium-Lead Blanket Design Studies for DEMO Reactor: Definition and Recent Developments of the Box-Shaped Concept," *Fusion Tech*., **21**, 2081 (1992).

13. S. MALANG, R. MATTAS, "Comparison of Lithium and the Eutectic Lead–Lithium Alloy, Two Candidates Liquid Metal Breeder Materials for Self-Cooled Blankets," *Fusion Eng. Des*., **27**, 399 (1995).

14. S. SMOLENTSEV, N. VETCHA, R. MOREAU, "Study of Instabilities and Transitions for a Family of Quasi-Two-Dimensional Magnetohydrodynamic Flows Based on a Parametric Model," *Phys. Fluids*, **24**, 024101 (2012).

15. I. MELNIKOV, N. RASUVANOV, V. SVIRIDOV, E. SVIRIDOV, A. SHESTAKOV, "An Investigation of Heat Exchange of Liquid Metal during Flow in a Vertical Tube with Non-Uniform Heating in the Transverse Magnetic Field, *Thermal Engineering*, **60**, 355 (2013).

16. I. KIRILLOV et al., "Buoyancy Effects in Vertical Rectangular Duct with Coplanar Magnetic Field and Single Sided Heat Load," *Fusion Eng. Des*., **104**, 18 (2016).

17. I. BELYAEV et al., "Temperature Fluctuations in a Nonisothermal Mercury Pipe Flow Affected by a Strong Transverse Magnetic Field," *Int. J. Heat Mass Transfer*, **127**, 566 (2018).

18. S. SMOLENTSEV, R. MOREAU, M. ABDOU, "Characterization of Key Magnetohydrodynamic Phenomena for PbLi Flows for the US DCLL Blanket," *Fusion Eng. Des*., **83**, 771 (2008).

19. N. VETCHA, S. SMOLENTSEV, M. ABDOU, R. MOREAU, "Study of Instabilities and Quasi-Two-Dimensional Turbulence in Volumetrically Heated MHD Flows in a Vertical Rectangular Duct," *Phys. Fluids*, **25**, 024102 (2013).

20. X. ZHANG, O. ZIKANOV, "Mixed Convection in a Downward Flow in a Vertical Duct with Strong Transverse Magnetic Field," arXiv preprint arXiv:1804.02659, 2018.

21. O. ZIKANOV, Y. LISTRATOV, "Numerical Investigation of MHD Heat Transfer in a Vertical Round Tube Affected by Transverse Magnetic Field," *Fusion Eng. Des*., **113**, 151 (2016).

22. F.R. URGORRI et al., "Magnetohydrodynamic and Thermal Analysis of PbLi Flows in Poloidal Channels with Flow Channel Insert for the EU-DCLL Blanket, *Nuclear Fusion*, **58**, 106001 (2018).

23. S. SMOLENTSEV et al., "MHD Thermohydraulics Analysis and Supporting R&D for DCLL Blanket in the FNSF," *Fusion Eng. Des*. **135**, 314 (2018).

24. S. SMOLENTSEV et al., "Construction and Initial Operation of MHD PbLi Facility at UCLA," *Fusion Eng. Des*., **88**, 317 (2013).

25. T. RHODES, G. PULUGUNDLA, S. SMOLENTSEV, M. ABDOU, "3D Modelling of MHD Mixed Convection Flow in a Vertical Duct," *Fusion Eng. Des*. Submitted, 2019.

26. Introduction to COMSOL Multiphysics, Version: COMSOL 5.4, 2018.

27. ANSYS Fluent Theory Guide, ANSYS Inc, Release 15.0, November 2013.

28. A. TASSONE, "Study of Liquid Metal Magnetohydrodynamic Flows and Numerical Application to a Water-Cooled Blanket for Fusion Reactors," Ph.D. Thesis, Sapienza University of Rome, March 2019.

29. C. MISTRANGELO, L. BÜHLER, "Development of a Numerical Tool to Simulate Magnetohydrodynamic Interactions of Liquid Metals with Strong Applied Magnetic Fields," *Fusion Sci. Tech*., **60**, 798 (2011).

30. S. SMOLENTSEV, N. VETCHA, M. ABDOU, "Effect of a Magnetic Field on Stability and Transitions in Liquid Breeder Flows in a Blanket," *Fusion Eng. Des*., **88**, 607 (2013).

31. A. PATEL et al., "Validation of Numerical Solvers for Liquid Metal Flow in a Complex Geometry in the Presence of a Strong Magnetic Field," *Theor. Comput. Fluid Dyn*., **32**, 165 (2017).